SANDIA REPORT SAND86—0033 • Unlimited Release • UC—45
Printed June 1986

Detonation Cellular Structure and Image Processing

J. E. Shepherd, S. R. Tieszen

Prepared by
Sandia National Laboratories
Albuquerque, New Mexico 87185 and Livermore, California 94550
for the United States Department of Energy
under Contract DE-AC04-76DP00789

Issued by Sandia National Laboratories, operated for the United States Department of Energy by Sandia Corporation.

Printed in the United States of America
Available from
National Technical Information Service
U.S. Department of Commerce
5285 Port Royal Road
Springfield, VA 22161

NTIS price codes
Printed copy: A03
Microfiche copy: A01

Distribution
Category UC-45

SAND86-0033

Detonation Cellular Structure and Image Processing

J. E. Shepherd and S. R. Tieszen

Sandia National Laboratories
Albuquerque, NM 87185

Abstract

Gaseous detonations universally exhibit an instability that is manifested as cellular patterns on witness plates (sooted foils) or open shutter photographs. The characteristic dimension or cell width λ of the periodic cellular pattern has previously been shown to correlate with failure diameter, critical diffraction aperature dimension and direct initiation energy requirements. Due to the importance of predicting these parameters in assessing detonability hazards, a quantitative method for cell size measurement is urgently needed. We discuss a technique based on digital image processing of sooted foil records and illustrate the results with data from experiments performed in the Heated Detonation Tube facility at Sandia. We demonstrate that image processing can be used to eliminate some of the uncertainty now present in cell size measurements. The possibility of quantifying cellular irregularity is also explored.

Contents

List of Figures

1 Introduction

Gas–phase detonation physics has been extensively investigated over the last three decades for a variety of fuel–oxidizer combinations. Recent investigations[1] have led to the conjecture that detonation limits are characterized by a set of universal relations between the detonation cell width λ and the physical dimensions of the experimental apparatus. Examples of this behavior include the critical tube size correlation[2] $d_c = 13\lambda$, the failure diameter correlation[3] $d_f = \pi\lambda$, and the critical initiation energy criterion[4] $E_c = 480\rho_\circ U_{CJ}^2\lambda^3$.

If these correlations are indeed universal, a powerful and inexpensive method of detonability assessment is at hand. Expensive and time–consuming large–scale tests for fuel–air mixtures, required because of the large values of d_c and E_c for insensitive mixtures, could be replaced by inexpensive and much simpler laboratory–scale measurements of cell size. Development of detailed chemical kinetics models for the oxidation of many fuels and the increasing reliability of numerical predictions of cell size[5,6] suggest that detonability estimates could be made numerically in some cases.

However, there are two serious deficiencies in relying solely on cell size to determine detonability. First, as pointed out by Lee,[1] cell size measurement is an art rather than a science and an experienced observer is needed to obtain consistent results. Sooted foils often exhibit a bewildering range of length scales and substantial irregularity in the overall quasiperiodic pattern. Often, even experienced observers will disagree on the choice of a dominant transverse wavelength by a factor of 2 or more. This subjectivity must be removed before cell size can be used in a quantitative fashion.

Second, it may not be possible or adequate to characterize most cellular structures by a single parameter. Experimental evidence[7] indicates that irregularity is an intrinsic feature of many fuel–air detonation cellular structures. The very regular structures observed in some experiments[8] appear to be the exception rather than the rule. Irregularity has a physical origin and is apparently most prominent in those mixtures that have a high sensitivity of reaction zone length to variations in shock strength.[9] In order to characterize irregular structures, some statistical or probabilistic methods must be used to describe the cell size distribution or its moments.

In order to resolve both issues mentioned above, a quantitative and objective means of assessing cell size must be developed. The present paper discusses the application of digital image processing to cellular patterns and develops a methodology for characterizing cell size in an objective manner. The influence of various sources of noise and irregularity are studied with the aid of synthetic images generated in both one and two dimensions. Results are given for experimental records of hydrogen–air detonations and compared with the more conventional methods of cell size measurement.

2 Detonation Cellular Structure

A typical sooted foil record from a detonation experiment is shown in Fig. 1. As described below in the experimental section, this record was obtained by placing a carefully sooted sheet of metal inside a detonation tube with the sooted side facing inward. The gas was then detonated at the opposite end of the tube and the detonation wave propagated over the foil from left to right. The foil was retrieved from the tube after the experiment and photographed in order to obtain the image shown here.

The cellular pattern shown in Fig. 1 is created by the triple points formed by the intersection of the main detonation wave with the transverse secondary shocks. The geometry of the wave interactions and the trajectory of the triple points is shown in Fig. 2 for a planar wave system. The transverse waves are a universal feature of gas–phase detonations and appear as a result of the intrinsic instability of the chemically reacting, gasdynamic flowfield constituting the detonation. There are two sets of these transverse waves corresponding to the two independent transverse directions for wave propagation behind the main shock.

For detonations confined in a circular tube, these two sets correspond to clockwise and counterclockwise rotating disturbances. Viewed from the laboratory, the triple points trace out helical paths on the interior of the tube. If we "unroll" the surface of the tube, corresponding to viewing an unrolled sooted sheet inserted into the tube, each triple–point will appear to trace out an almost straight line path on the surface at an oblique angle to the direction of detonation propagation. Considering the triple–point paths produced by the periodically spaced transverse waves of both families yields the cellular pattern sketched in Fig. 3a. It is this pattern that is displayed in Fig. 1.

The curvature of the triple–point paths shown in Fig. 3a is exaggerated and more appropriate for a fuel–oxygen mixture than for fuel–air mixtures. For fuel-air detonations, the transverse waves are much weaker (Mach number $M \sim 1.2$) than the main shock ($M \sim 5$) and can be loosely thought of as strong acoustic disturbances. If the strength of both the main and transverse shock waves can be approximated as constant throughout the cell, then the track of the triple–point lies at a fixed angle with respect to the direction of propagation and the triple–point paths are straight lines. We will utilize this idealization later in the construction of synthetic images that simulate actual cellular patterns from detonations.

2.1 Conventional Cell Size Measurements

Previous work characterizing cellular structure has concentrated on determining a single parameter, the so–called detonation cell width indicated by the distance λ in Fig. 3. The traditional measurement technique is for one or more experimenters to view the sooted foil and on the basis of experience, to choose a single distance characteristic of the dominant or average spacing.

Two methods exist[10] for deciding what represents the dominant spacing. One method is to select the diamond patterns which have a regular shape and a high–

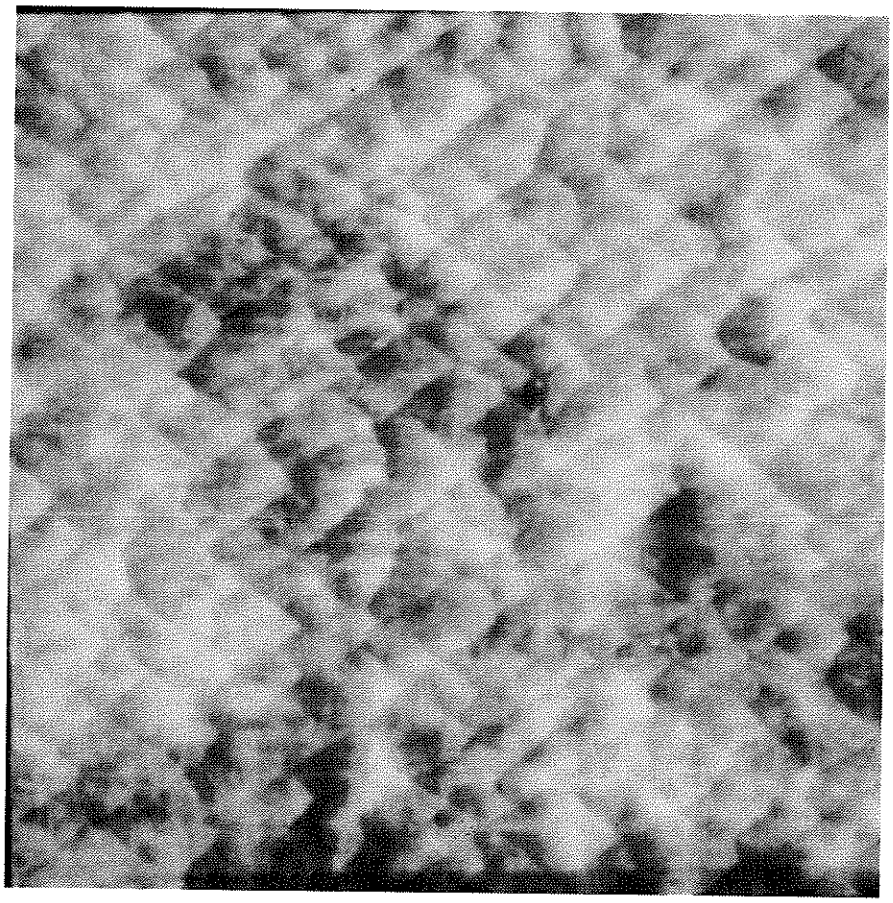

Figure 1: Digitally enhanced photograph of a sooted foil obtained in HDT test HT95 with a hydrogen–air mixture. Initial conditions of 293 K, air density of 41.6 mole/m^3, and equivalence ratio $\phi = 0.5$.

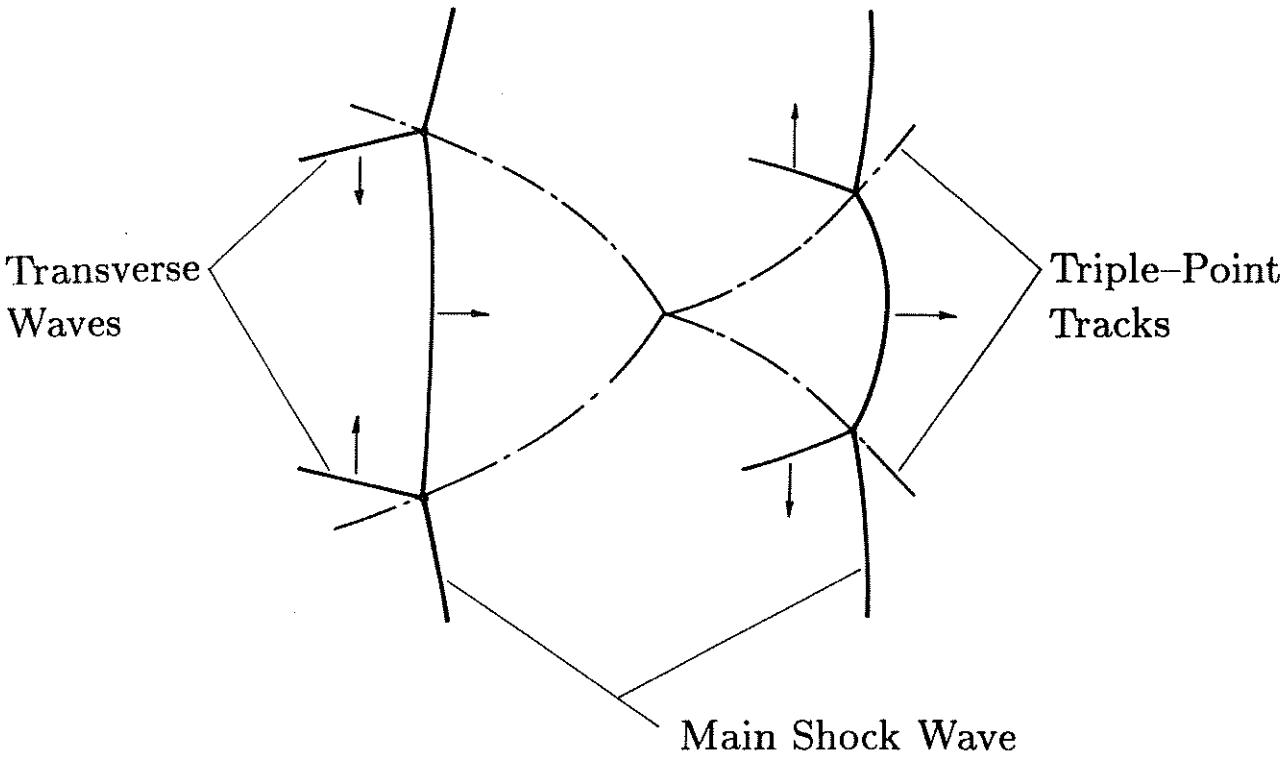

Figure 2: Schematic of the triple-point tracks and the transverse shock motion required to produce them.

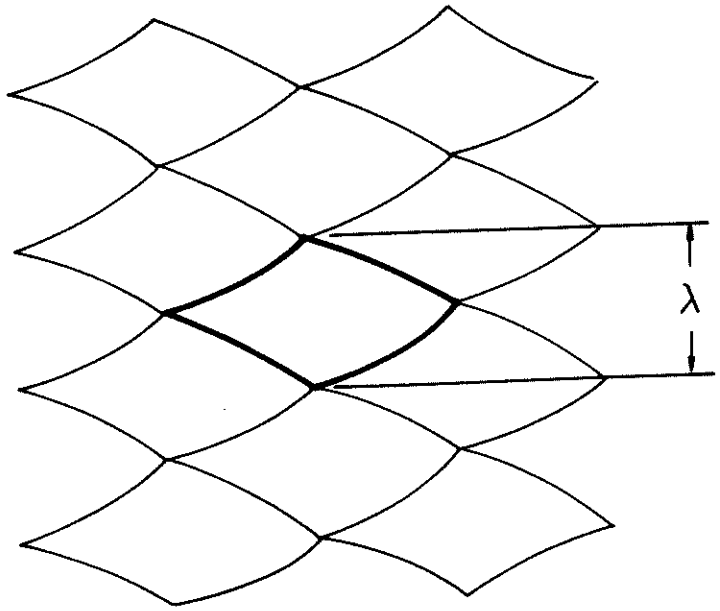

(a)

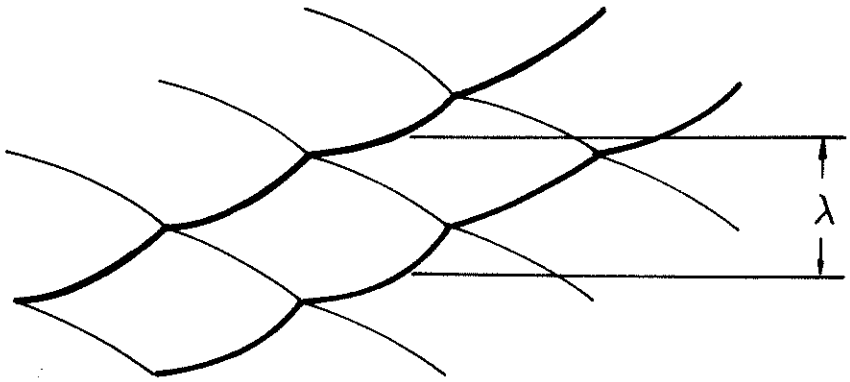

(b)

Figure 3: Conventional measures of the detonation cell width. (a) Diamond pattern analysis. (b) Track spacing analysis.

contrast ratio between the triple–point tracks and the background soot. The width between the vertices of the diamonds is chosen to be the cell spacing λ. An idealized diamond is shown in Fig. 3a.

The second method, more commonly used, selects strong (*i.e.*, high–contrast ratio) long-running (*i.e.*, existing for many cell widths) parallel triple–point tracks. The cell width is the distance between tracks measured perpendicular to the direction of detonation propagation. A pair of these tracks is indicated in Fig. 3b. There are two criteria in selecting appropriate tracks. One is the length of the line relative to the measured width between the parallel lines and the other is the contrast ratio between the tracks and the background.

These methods are perfectly adequate as long as the cellular structure is reasonably periodic and the associated track spacing is unambiguous. Unfortunately, this is not the case for fuel–air detonations. As seen in Fig. 1, the cellular pattern is only quasiperiodic and several possible spacings are observed. In such cases, both methods become highly subjective and regardless of the method chosen, substantial ambiguity exists in the derived detonation cell width.

3 Image Processing Analysis

In order to eliminate the ambiguity in cell size measurement, we have developed a technique based on digital image processing to characterize the cellular patterns observed on sooted foils. Before discussing the application of this method to actual data, we will illustrate the general concepts using an idealized cellular pattern and synthetically generated images.

3.1 Ideal Synthetic Images

An idealized cellular pattern is shown in Fig. 4a. In the language of signal processing, this image can be decomposed into two independent, periodic "wavetrains." The normals to the wavefronts are oriented at angles $\pm\alpha$ with respect to the x–axis, the direction of detonation propagation. Consider one of these wavetrains and its one–dimensional projection[a] onto the line $\mathbf{X}_\alpha$, which is parallel to the normals to the wavefronts. For this special case, all the information about the wavetrain is contained in this one–dimensional projection.

One possible idealized representation of this projection is the series of periodically spaced, rectangular pulses shown in Fig. 4b. The actual image may have a very different representation but by suitable preprocessing steps (described below) it is often possible to transform the image into a signal resembling this simple shape.

How can we characterize this pattern using image–processing methods? A natural technique to investigate is Fourier (spectral) analysis. From classical signal–processing

[a] A projection is defined here to mean the one–dimensional signal that results when evaluating a two–dimensional signal along a specified direction or line.

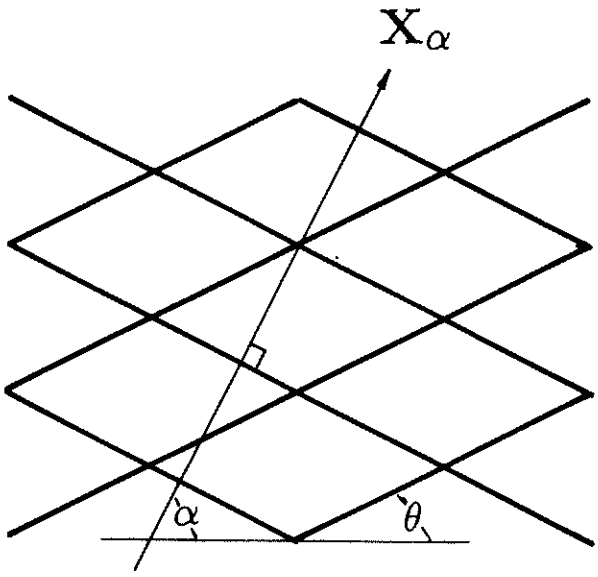

(a)

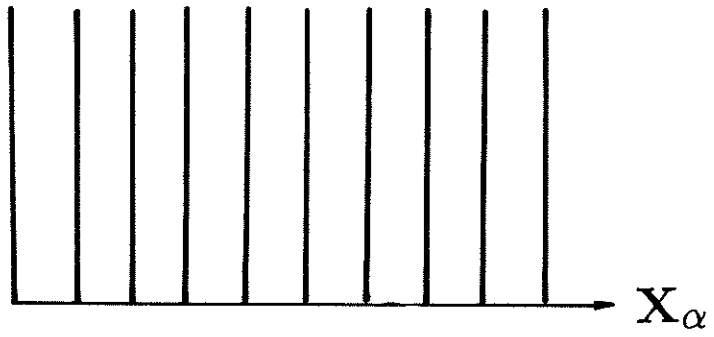

(b)

Figure 4: Synthetic, perfectly periodic cellular structure. (a) Two-dimensional pattern. (b) One-dimensional projection of image intensity from a single family of tracks onto a normal direction $\mathbf{x}_\alpha$.

theory we know that any periodic component of a signal will show up as a peak in the Fourier spectrum. Using a two–dimensional implementation of the Fast Fourier Transform (FFT), we have computed the spectrum of the synthetic signal shown in Fig. 4a.

In accord with standard signal–processing practice, we will work with the power spectral density (PSD), which is the absolute square of the amplitude of the Fourier coefficients. The logarithm of the PSD derived from Fig. 4a is rendered as a gray scale image in Fig. 5a. High values of the PSD are rendered as white tones, low values as black, and a continuous variation of gray levels exists corresponding to the magnitudes in between. The magnitude of the PSD at a given wavelength can be thought of as the amount of "power" in the original image that is concentrated at that wavelength.

Note that except for some leakage, the power is concentrated into discrete points located along two bands forming the central "X" in Fig. 5a. The orientation of each leg of the "X" coincides with the normals to the wavetrains, one of which is shown in Fig. 4a. This is a reflection of the nature of the original image, a superposition of two one–dimensional, obliquely oriented wavetrains. In this idealized case of perfectly periodic, one–dimensional images, the resulting PSD is particularly simple.

Each wavetrain has a one–dimensional Fourier transform which is identical to the projection of the two–dimensional transform onto the preferred directions $\pm\alpha$. In the present case, the projection of the transform onto one of the normal directions is shown in Fig. 5b. The long wavelength modulation shown in Fig. 5b is due to the rectangular pulse structure of the lines themselves; the shorter wavelength peaks occur at multiples of the frequency of interest, *i.e.*, the reciprocal of the intertrack spacing.

This idealized example of a cellular structure is very instructive and is quite useful in understanding the PSD obtained from actual data such as Fig. 1. As discussed later, the main features such as the central "X" and the peaks in the PSD corresponding to the dominant spacings are observed in the PSDs obtained from the data. However, there are several key ways in which the data differ from these synthetic images. Actual detonation cellular structures are: a) not perfectly periodic, *i.e.*, there is some random variation in the track-to-track spacing; b) not one-dimensional, *i.e.*, the tracks have a finite length and the track orientation has some random variation; c) not always capable of being transformed into a wavetrain of uniform rectangular pulses, *i.e.*, there may be background noise present and some random variation in the pulse height and width. These nonideal features are discussed next.

3.2 Nonideal Synthetic Images

All of the nonideal aspects of actual data can be studied by adding imperfections to the idealized pattern discussed above. Due to our ignorance of the detailed physical processes that produce the actual cellular patterns, we will assume that the imperfections have a random character and can be modeled as such. Associated with each type of imperfection is a probability distribution function (pdf) for the feature we have chosen to be a random variable. The degree of randomness produced by that feature

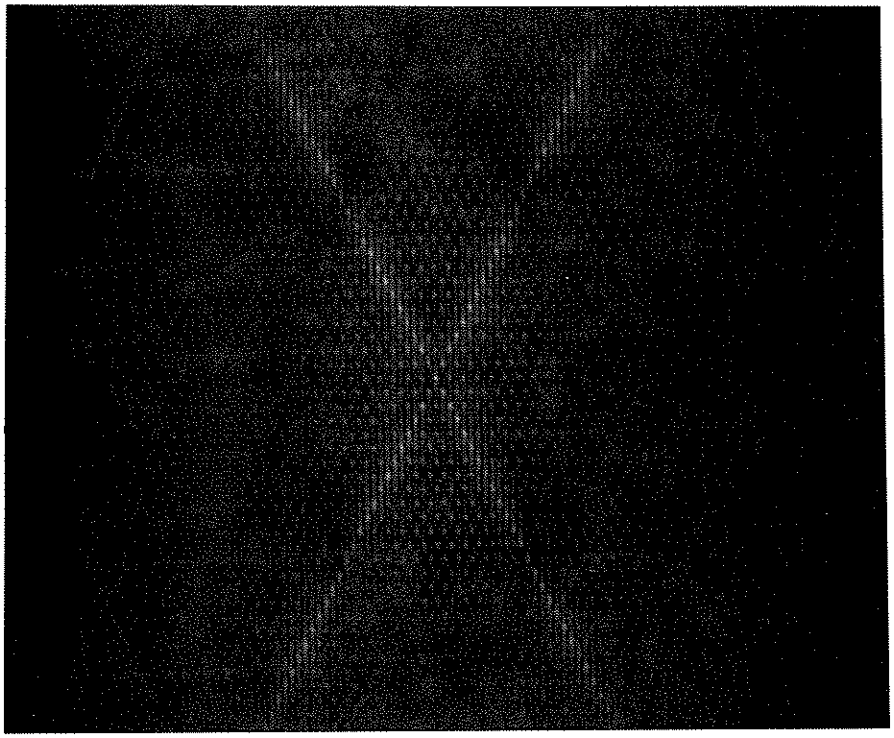

(a)

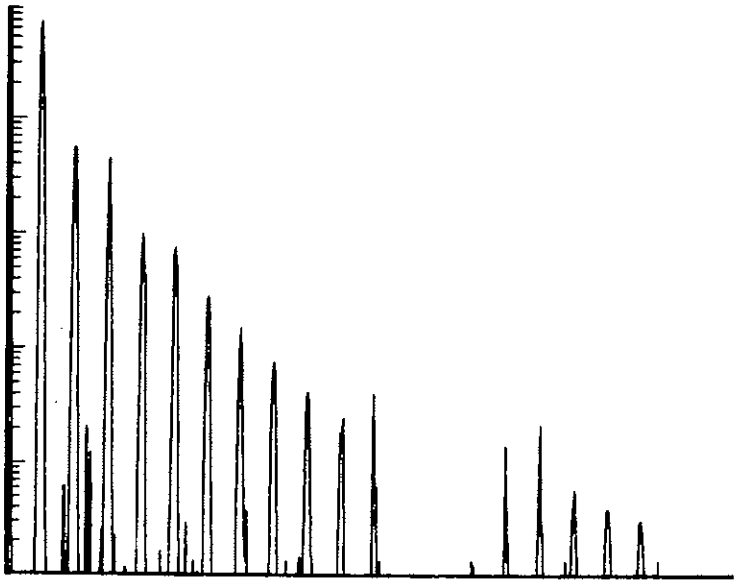

(b)

Figure 5: Fourier transform of perfectly periodic synthetic image. (a) Gray level representation of power spectral density (PSD). (b) Projection of PSD along a principal axis, *i.e.*, one of the legs of the "X".

can be quantified in terms of the values of the parameters (mean, variance, *etc*) entering into the pdf. At present, these parameters are rather arbitrary and are chosen to yield a qualitative resemblence to actual data. As our understanding of detonation instability improves, these *ad hoc* assumptions about the nature of the cellular structure can be replaced with more reasonable, physical constraints.

The effects of the various types of nonideal behavior have been investigated in two ways. First, we have performed numerical experiments on synthetic images which contain features determined by stochastic functions approximated by the appropriate psuedo-random-number sequences. Second, we have used analytical methods based on the theory of stochastic processes and reasonable assumptions about the behavior of ensemble averages of nonideal, stochastic cellular patterns. Since we have focused on the PSD to quantify cellular patterns, the effect on the PSD of each type of imperfection mentioned above is summarized separately below.

All of the types of nonideal behavior contribute to what has been termed the irregularity of the cellular structure. In a simplified manner, we have attempted to classify these sources of nonideal behavior from a signal processing point of view. What we have not done in this paper is to relate our description to observations on physical systems.[b] This will require a much more detailed and systematic study on cellular patterns of varying degree of regularity. Another important aspect we do not discuss is the application of statistical methods to derive the parameters of the governing pdf's.

3.2.1 Averaging and PSD Computations

Before discussing the PSD of stochastic images, it is necessary to refine our computing technique somewhat. It is well known that power spectral density estimates for noisy data cannot be reliably made from a single Fourier transform. The signal–to–noise ratio (S/N) in the resulting PSD is quite low and the confidence intervals on the location of the spectral peaks will be very large.[11] In order to make reliable spectral estimates, the PSD's of an ensemble of images have to be averaged together. The confidence interval on the average PSD amplitudes decreases exponentially with the number of independent samples for a fixed number of frequency bands in the spectra.[11]

Ideally, the images in the ensemble are obtained from independent or non-overlapping sections of the sooted plate. A practical technique that requires less work is to use an ensemble of partially overlapping subimages from a single image. The improvement in S/N is not as large as if the images were independent but a significant increase is still possible. In the present work, averages from 9 subimages that are each 1/4 of the area of the original image and overlap each other by 50% were used to compute the PSD's of both actual and noisy synthetic data.

A further complication with the present data is that the images are quite coherent in one direction, *i.e.*, there is a high degree of correlation in the direction parallel to the triple–point tracks. This lack of statistical independence is greatest in the track

[b] A first attempt to do this for detonations in Ar-diluted H_2-O_2 and C_2H_2-O_2 is being pursued in a joint effort between Sandia National Laboratories and Defense Research Establishment Suffield.

patterns that are closest to the idealized one-dimensional images discussed above. This coherence means that even less improvement in S/N is realized. The limiting case is that for perfectly one–dimensional signals, no gain at all is realized by averaging. This issue of partial coherence and the effect on the averaging process and the power spectral density is quite complex and not fully resolved at the present time.

Averaging has only a small effect on one–dimensional projections of PSDs derived from images of actual detonation cellular structures. This is a consequence of the projection theorem: Evaluating a two–dimensional spectrum along a line is equivalent to averaging the image in space perpendicular to that line and then performing a one-dimensional transform.[12] The averaging process implied by this theorem already provides a substantial increase in S/N since there are a large number (~ 512) of "samples", *i.e.*, pixels in the direction perpendicular to the tracks. to computing averaging the a given family

3.2.2 Track Spacing Randomness

The imperfections observed in actual cellular patterns result in a degradation in the sharpness and number of the individual peaks observed in the projected spectrum shown in Fig. 5b. The larger the variance in the intertrack spacing, the fewer number of peaks are present in the spectrum. For a large enough variance, only a single peak centered around the principal spacing will be observed. We have modeled this effect using both synthetic images and analytic methods. Our results indicate that it is probably the most important type of nonideal behavior present in the images.

3.2.3 Finite Track Length and Orientation Variation

Deviations from one-dimensional behavior result in a transverse broadening of main power bands (the central "X" in Fig. 5a) in the PSD. The shorter the track length or the greater the variance in track orientation angle θ, the broader the bands. Randomness in orientation produces a wedge–shaped band; finite track length uniformly broadens the band. The S/N of the projected PSD will also be decreased since the transverse correlation length of the wavetrains is decreased by both processes. This is the next most important type of nonideal behavior in the images.

3.2.4 Amplitude Noise

Random variations in the amplitude of the pulses and/or a noisy background image will decrease the S/N of the projected spectrum. Randomness in the width of the tracks results in a broadening of the spectral peaks observed in the projected PSD. This is the least important type of nonideal behavior present in the images.

4 Heated Detonation Tube Experiments

The image–processing analysis described above for the synthetic images was applied to real sooted foil images taken from five tests conducted in the 0.43 m diameter Heated Detonation Tube or HDT.[13] These tests were made as part of a series of hydrogen-air detonation sensitivity tests with application to nuclear-reactor safety. The test conditions for the five tests are an initial temperature of 293 K, an initial air density of 41.6 moles/m^3 (*i.e.*, an air pressure of 1 atm at 293 K), and equivalence ratios of 0.4, 0.5, 0.6, 0.8, and 1.0.

The detonation cell tracks were recorded on 1.22 m wide by 3.66 m long aluminum sheets that were sooted with a MAPP (Stabilized Methylacetylene–Propadiene) gas torch using ambient air as the oxidizer. The soot was applied to these large sheets by suspending the sheets horizontally in a frame over the torch while the torch was moved back and forth. The sooted sheets were rolled into a cylinder and inserted into the end of the HDT with the unsooted side flush against the inner surface of the detonation tube wall.

One disadvantage of sooting a plate in this manner is it is very difficult to obtain a uniform coating of soot on the plate, particularly for large plates. Many particle coatings which can be applied more uniformly than soot have been tried without much success, and therefore, most researchers today use the sooted plate technique to record detonation cell width.

The sooted aluminum sheets from the five tests were photographed with Kodak Technical Pan Film using a 50 mm square negative format. The film grain size is less than 5-10 μm. The photographs were taken so that the final digitized image would be approximately 5 to 10 detonation cells in width. For the leanest test, the final image was only 3 or 4 detonation cell widths across because of the large width of the detonation cells ($\sim$ 400 mm) relative to the size of the sooted aluminum sheet.

These negatives were then digitized using a Perkin–Elmer scanning microdensitometer which converts the scanned negative density to a gray level ranging from 0-255 in magnitude. At each scan position, a 50 μm spot size was used to obtain the gray level. The microdensitometer was moved in 50 μm increments to produce a 512 $\times$ 512 array covering 26 mm $\times$ 26 mm of the image on the negative.

4.1 Analyzing HDT Foils

One example of a digitized image from an HDT test is shown in Fig. 1. This image has already been enhanced over the original. Even with the high contrast film, the original negative only yields a narrow range of gray levels: 40 out of the possible range of 256. This low contrast will result in a poor S/N in the PSD. As part of the preprocessing operations performed on each digitized image, the contrast is expanded by applying a linear mapping to the gray level of each pixel of the image.

Following contrast enhancement, the gray levels along a line across the the middle of the image vary as shown in Fig. 6a. The sharp transitions between high and low

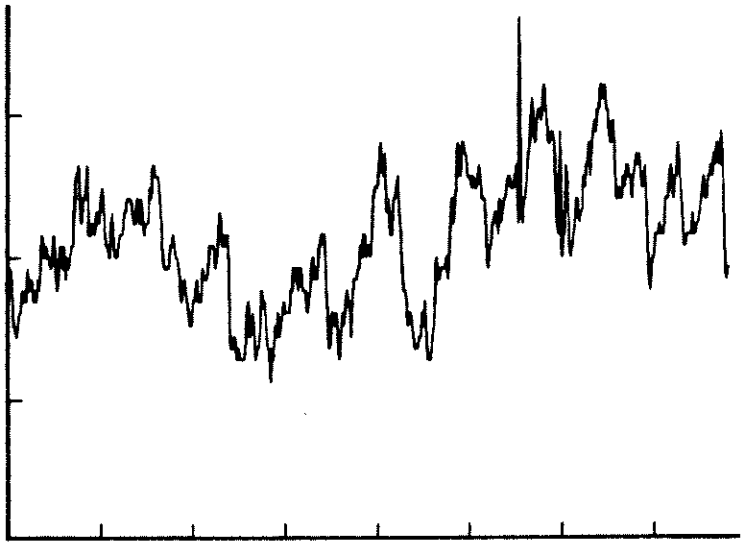

(a)

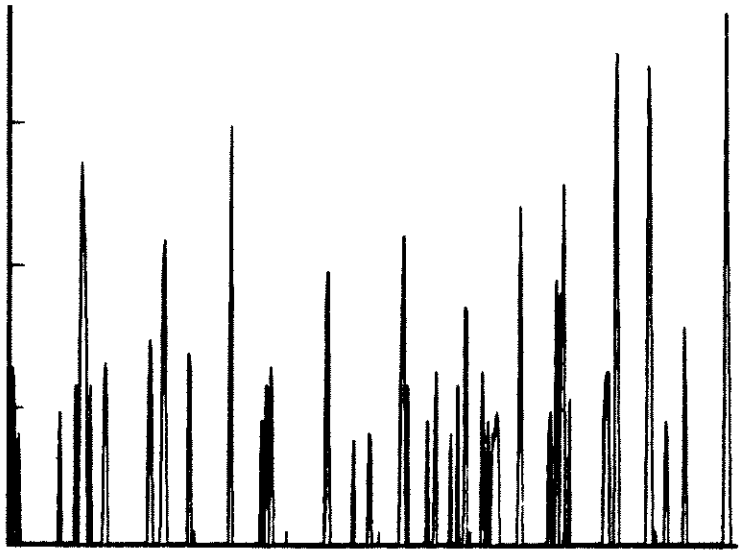

(b)

Figure 6: Gray scale values along a horizontal line across the middle of the image in Fig. 1. (a) Original image. (b) Image after processing with the Sobel edge operator.

gray levels correspond to the location of the triple–point tracks. The average value of the gray level appears to vary between the triple–point tracks in approximately the form of a ramp wave (with some superimposed noise). Also note that the average level or background shows a long wavelength variation. This is mainly due to nonuniformity in the smoking technique, or to a lesser extent, the nonuniformity of the lighting on the sooted sheet when photographed.

Usually the averaging consequences of the projection theorem minimize the effects of nonuniform intensity on the projected PSDs. However, in some cases the variations in background intensity are strong enough to produce spurious results in the PSD. In those instances, further preprocessing can be performed to eliminate the slowly varying background and emphasize the tracks. One class of techniques are edge–enhancement algorithms; these are analogous to finite difference operators and emphasize transitions. The effect of the Sobel edge operator[14] on the image scan line of Fig. 6a is shown in Fig. 6b. The background variation has been removed and the triple–point tracks now correspond to pulses as opposed to ramp wave transistions in the original image.

The PSD of the image shown in Fig. 1 is represented as gray levels in Fig. 7. The "X" pattern characteristic of the diamond pattern composed of two sets of parallel lines is clearly evident. Although each band forming the X is wider than the bands generated by the ideal synthetic image (see Fig. 5a), the narrowness of these bands indicates the one–dimensional nature of each family of triple–point tracks. This is also clearly visible in the original image; numerous tracks span almost the entire image. An angular scan at a fixed radius (corresponding to $1/4$ of the distance from the origin) is shown in Fig. 8 to emphasize the sharpness of these bands.

The location of the principal axes or legs of the X in the PSD are found by comparing the integrals of the spectral density along lines passing through the origin in the spectral plane. A well–defined maximum is obtained for each leg at a particular angle of orientation $\alpha_{\pm}$. The angles which the corresponding family of triple–point tracks make with respect to the direction of detonation propagation are $\theta_{\pm} = \pi/2 \mp \alpha_{\pm}$. For Fig. 7, these angles are $\theta_{+} = 32.2°$ and $\theta_{-} = -34.9°$.

These values are typical of all of the images we have analyzed. They are not equal and opposite since the foil and/or image is not precisely aligned with the axis of the HDT. A mean value of 34° for the track angle implies a transverse wave Mach number of ~ 1.2 if the equilibrium sound speed behind the detonation is used in the computation. This agrees with the strength of the transverse waves inferred by Strehlow and Biller[15] for "ordinary" detonations in fuel–oxygen mixtures diluted with argon. Note that the track angles computed for sound waves are less: $\sim 26°$ based on the frozen sound speed behind the shock; $\sim 29°$ based on the equilibrium sound speed. A track angle θ between $33° - 35°$ has been found by many other investigators and appears to be representative of "ordinary" detonations.

Projections of the PSD onto each leg of the X are shown in Fig. 9. The abscissa has been multiplied by $\sin\theta$ in order to directly compare these wavelengths with the standard cell width measurements as described in Fig. 3. Spectral peaks correspond to wavelengths of 155, 121, 98, and 68 mm. The large peak at zero frequency (not

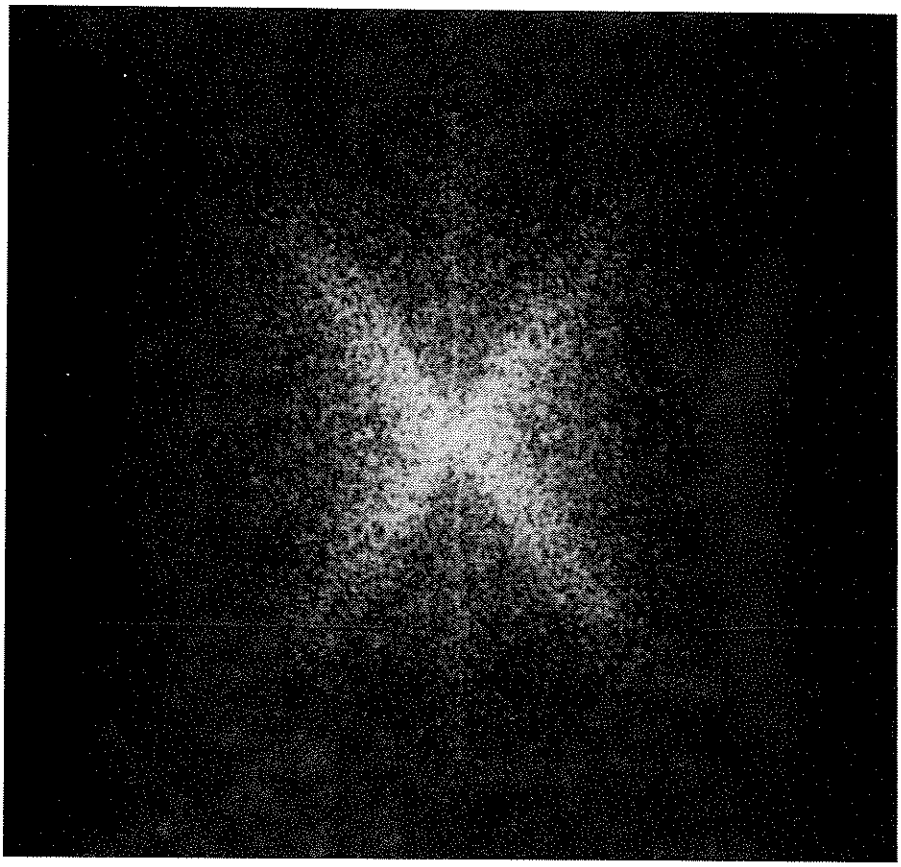

Figure 7: Gray level representation of the PSD of the image shown in Fig. 1. Logarithmic scaling used for clarity.

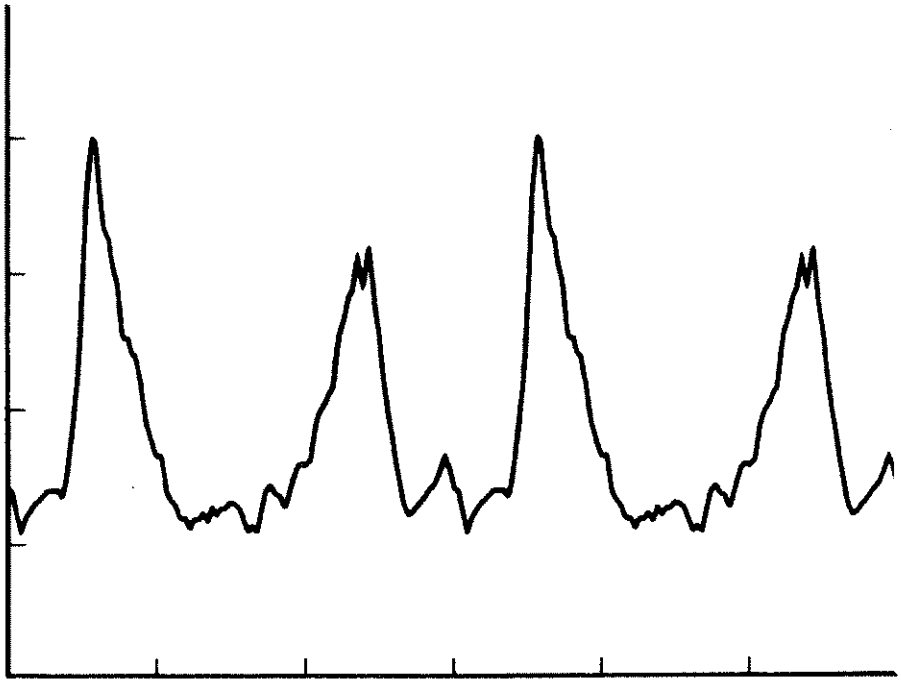

Figure 8: Angular scan at the 1/4 radius point of the PSD shown in Fig. 7. Peaks correspond to the locations of the legs of the "X" seen in Fig. 7.

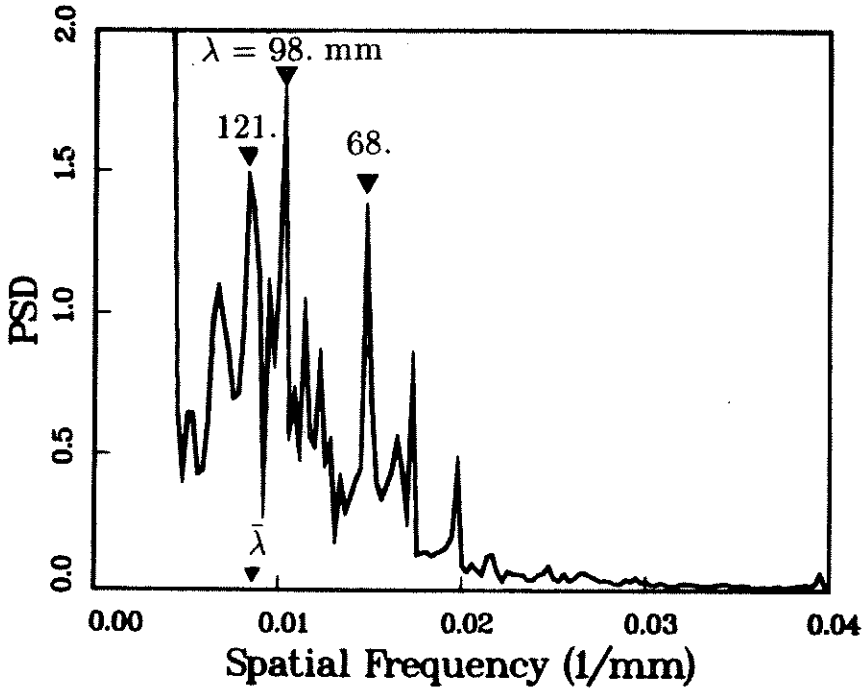

(a)

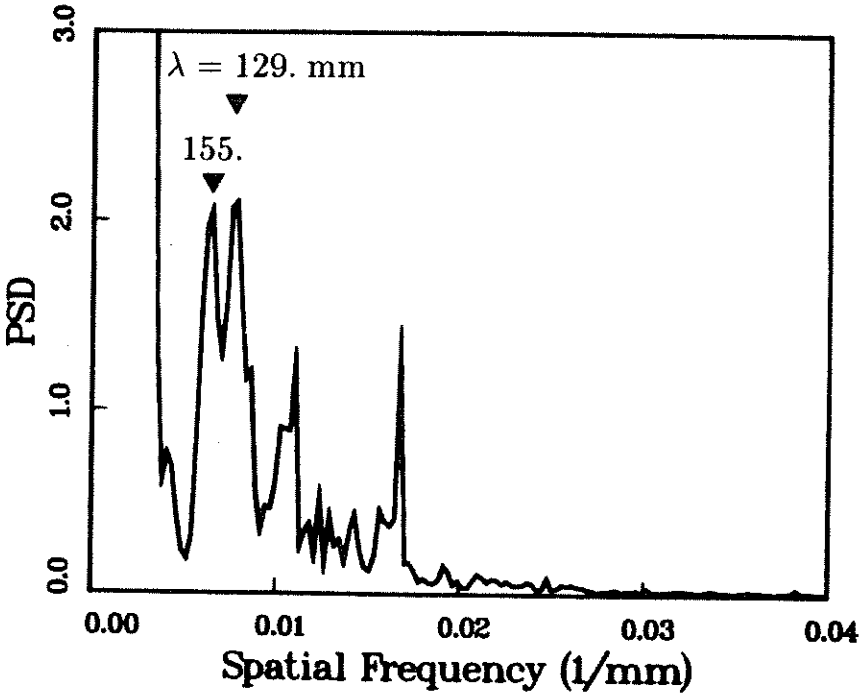

(b)

Figure 9: One-dimensional projections of the PSD shown in Fig. 7 onto the principal power axes, *i.e.*, the "X". (a) Projection corresponding to $\theta = 32.2°$. (b) Projection corresponding to $\theta = -34.9°$.

completely shown) is present because the sum of the gray levels is nonzero, *i.e.*, there is a net DC offset. The best estimate of detonation cell width by traditional measurement techniques is 115 mm. The location of the peak power in the spectrum is between 95-150 mm, in good agreement with the visual estimate. Note that the two projections have a significantly different frequency content. This indicates, in agreement with visual inspection of Fig. 1, that the two families of transverse waves have very different characteristics

The images from four other HDT tests were processed in the manner discussed above. These images were all either of the same quality or poorer than the example (test HT95) discussed above. However, in all cases it was possible to identify clear peaks in the spectrum and the location of the peak PSD was in good agreement with the visual estimate. The results of analyzing images from all 5 HDT tests are given in Table I. A comparison between the dominant wavelengths determined by the present spectral method and the previous visual estimates is shown in Fig. 10. The location of all major peaks in the spectra of both families of transverse waves are shown in Fig. 10. In order to compare with the previous visual results, the location of the largest peak is also given in Table I.

The good agreement shown in Fig. 10 between the present results and the previous estimates indicate that this new technique can replace the traditional visual estimates for determiming cell widths *and* can provide an objective and quantitative characterization of detonation cellular structure. While much more research is needed to reach the final goal, the potential has been demonstrated.

Table I
Summary of HDT Test Analyses

Test	ϕ	θ_+	θ_-	$\bar{\lambda}$ (mm)	λ^* (mm)	λ_i (mm)
HT92	1.0	34.3	-34.6	10	10.6	10.6, 5.1, 4.5
HT93	0.8	36.2	-32.8	13	20	48, 30, 20, 19, 14
HT94	0.6	33.6	-33.1	30	32	73, 50, 42, 32
HT95	0.5	32.2	-34.9	115	121	155, 129, 121, 98, 68
HT96	0.4	34.8	-38.3	400	385	385, 364, 183

ϕ Equivalence ratio
$\theta_\pm$ Track angles
$\bar{\lambda}$ Visual estimate
λ^* Spectral analysis (dominant peak)
λ_i Spectral analysis (all peaks)

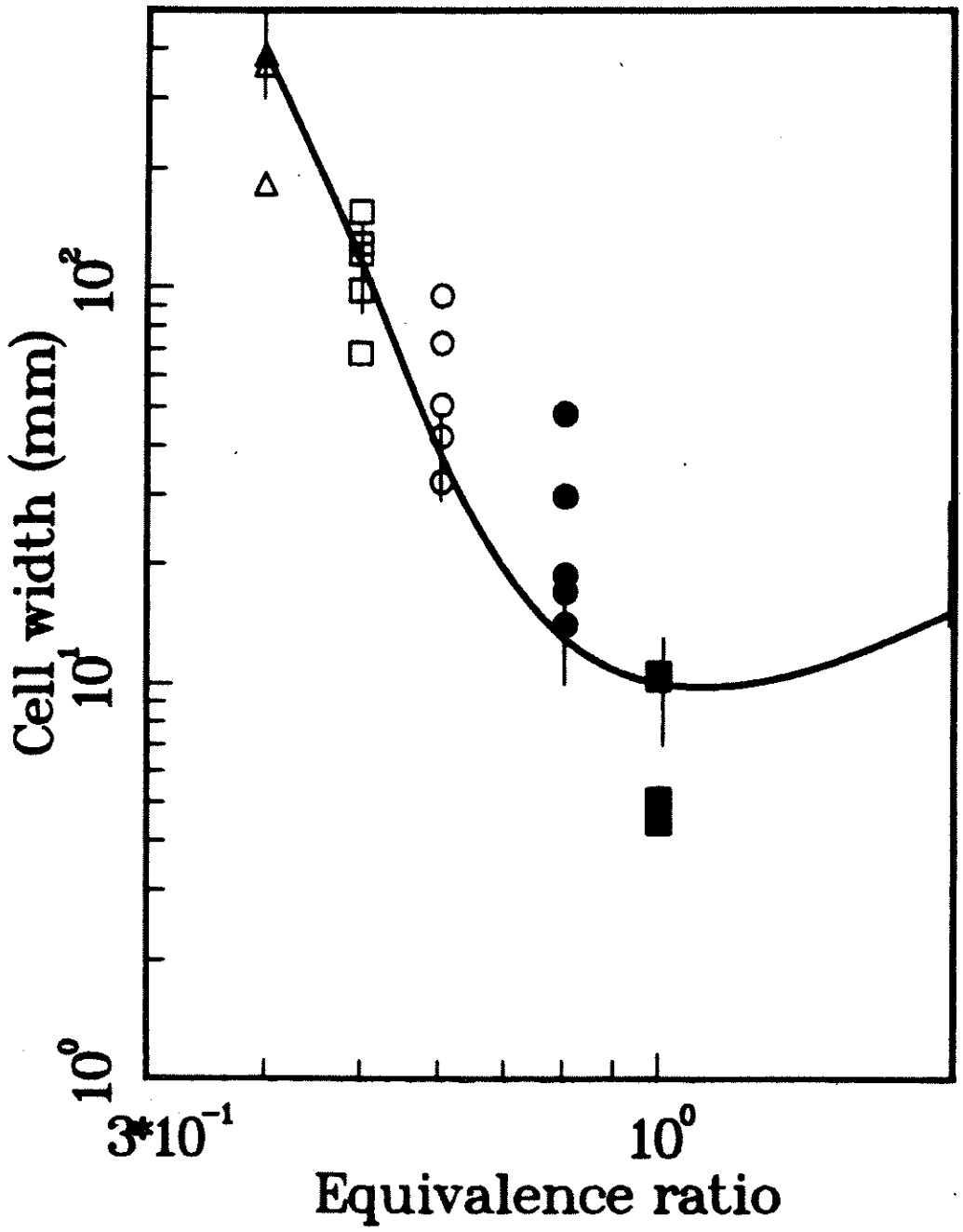

Figure 10: Comparison of the image–processing results with the previous results obtained by visual inspection. Solid line is a fit to the visual estimates discussed in Ref. 13. Vertical lines indicate the range of λ obtained by three independent observers. Data points correspond to the location of spectral peaks obtained by the methods described in the present report.

5 Conclusions

We have developed a digital image–processing technique for characterizing detonation cellular structure. This technique uses traditional image–processing methods and two–dimensional spectral analysis to obtain the power spectral density of the cellular patterns. The dominant cell width can be obtained directly from a one–dimensional projection of the spectral density. Numerical experiments with synthetic images demonstrate the ability of this method to determine both the dominant cell width and the degree of perfection or regularity of the cellular pattern. Analysis of images from 5 H_2-air detonation tests demonstrates the practicality of the method. Dominant cell widths obtained by the present technique overlap those obtained by more traditional methods. In addition, the present technique has the potential to completely quantify all aspects of the cellular patterns.

Acknowledgments

We thank Walter Dickenman for his efforts in photogaphing the sooted foils; Art McCarthy and Bob Hughes for performing the digitizing; Gary Mastin and Dennis Ghiglia for assistance with the image–processing programs. This work was supported by the U.S. Nuclear Regulatory Commission and performed at Sandia National Laboratories which is operated for the U.S. Department of Energy under contract number DE-AC04-76DP00789.

6 References

1. Lee, J. H.: Ann. Rev. of Fluid Mech. 16, 311, 1984.

2. Knystautas, R., Lee, J. H., and Guirao, C.: Combust. Flame 48, 63, (1982).

3. Moen, I. O., Donato, M., Knystautas, R. and Lee, J. H.: Eighteenth Symposium (International) on Combustion, p. 1615, The Combustion Institute, 1981.

4. Knystautas, R., Guirao, C., Lee, J. H. and Sulmistras, A.: Dynamics of Shock Waves, Explosions, and Detonations, p. 23, Progress on Astronautics and Aeronautics, 94, 1984.

5. Westbrook, C. K. and Urtiew, P. A.: Nineteenth Symposium (International) on Combustion, p. 615, The Combustion Institute, 1982.

6. Shepherd, J. E.: *Detonation Modeling and Reaction Kinetics in Hydrogen-Air-Diluent Mixtures.* Presentation at the Tenth International Colloquium on Dynamics of Explosions and Reactive Systems, Berkeley, CA, August, 1985.

7. Libouten, J-C., Dormal, M. and Van Tiggelen, P.J.: Proceedings of the First Specialist Meeting (International) on Combustion, p. 437, Bordeaux, France, July, 1981.

8. Strehlow, R. A.: Astronautica Acta 14, 539 (1969).

9. Moen, I. O., Sulmistras, A., Thomas, G. O., Bjerketvedt, D. and Thibault, P. A.: *The Influence of Cellular Regularity on the Behavior of Gaseous Detonations.* Presentation at the Tenth International Colloquium on Dynamics of Explosions and Reactive Systems, Berkeley, CA, August, 1985.

10. Moen, I. O., Murray, S. B., Bjerketvedt, D., Rinnan, A., Knystautas, R. and Lee, J. H.: Nineteenth Symposium (International) on Combustion, p. 635, The Combustion Institute, 1982.

11. Stearns, F. D.: Digital Signal Analysis, Hayden Book Co., Chap. 14, 1975.

12. Castleman, K. R.: Digital Image Processing, Prentice-Hall, p. 184, 1979.

13. Tieszen, S. R., Sherman, M. P., Benedick, W. B., Shepherd, J. E., Knystautas, R., and Lee, J. H.: *Detonation Cell Size Measurements in H_2-AIR-H_2O Mixtures.* Presentation at the 10th International Colloquium on Dynamics of Explosions and Reactive Systems, Berkeley, CA, August, 1985.

14. Ballard, D. H. and Brown, C. M.: Computer Vision, Prentice-Hall, p. 77, 1982.

15. Strehlow, R. A. and Biller, J. R.: Combust. Flame 13, 577 (1969).

DISTRIBUTION:

Unlimited Release
UC-45

DOE Albuquerque Operations Office
N. S. Dienes, Productions Operations Div.
Acting Director, Weapons Program Div.
Albuquerque, NM 87185

Combustion Dynamics, Ltd.
430 Sixth Avenue, SE
Suite 116
Medicine Hat, Alberta T1A 2S8
CANADA
P. A. Thibault

Department of Engineering Sciences
213 Aerospace Engineering Building
University of Florida
Gainesville, FL 32611
David Mikolaitis

Explosive Technology
P. O. Box KK
Fairfield, CA 94533-0659
J. E. Kennedy

Factory Mutual Research Corp.
P. O. Box 688
Norwood, MA 02062
R. Zalosh

Lawrence Livermore National Laboratory
P. O. Box 808
Livermore, CA 94550
E. L. Lee, L-368
W. J. Pitz, L-321
C. M. Tarver, L-368
P. A. Urtiew, L-368
C. K. Westbrook, L321

Lockheed EMSCO
P. O. Drawer MM
Las Cruces, NM 88004
C. V. Bishop
M. D. Pedley

Los Alamos National Laboratory
Los Alamos, NM
W. C. Davis, MS960
C. L. Mader, MS214
R. Rabie, M-9

McGill University
Mechanical Engineering Department
817 Sherbrooke
Montreal, Quebec
CANADA
J. H. Lee
R. Knystautas

Military Engineering Section
Defense Research Estab. Suffield
Ralston, Alberta T0J 2N0
CANADA
I. O. Moen
S. B. Murray

Dr. Roger Strehlow
505 South Pine Street
Champaign, IL 61820

University of Connecticut
Dept. of Mechanical Engineering
191 Auditorium Road
Storrs, CT 06268
Eli K. Dabora

University of Illinois
Dept. of Aeronautical and Astronautical Engineering
104 S. Mathews Avenue
Urbana, IL 61801

J. Buckmaster

University of Illinois
Dept. of Theoretical and Applied Mechanics
Urbana, IL 61801
D. Scott Stewart

University of Michigan
Dept. of Aerospace Engineering
Ann Arbor, MI 47109
Martin Sichel

1130 G. A. Samara
1131 B. Morosin
1131 W. B. Benedick
1131 B. Dodson
1131 R. A. Graham
1131 R. E. Setchell
1131 P. A. Taylor
1510 J. W. Nunziato
1512 J. C. Cummings
1512 J. E. Shepherd (5)
1513 D. W. Larson
1513 M. R. Baer
1520 D. J. McCloskey
1530 L. W. Davison
1534 J. R. Asay
1540 W. C. Luth
2644 D. C. Ghiglia
2644 G. A. Mastin
2515 A. M. Renlund
3141 S. A. Landenberger (5)
3151 W. L. Garner (3)
3154-1 C. H. Dalin (28) for DOE/OSTI
6420 J. V. Walker
6425 R. W. Ostensen
6427 M. Berman
6427 J. T. Hitchcock
6427 M. P. Sherman
6427 D. W. Stamps
6427 S. R. Tieszen (5)
8120 L. D. Bertholf

8244 R. J. Kee
8361 D. R. Hardesty
8523 B. R. Sanders

Org.	Bldg.	Name	Rec'd by	Org.	Bldg.	Name	Rec'd by

Sandia National Laboratories